The Seventh Asian-Pacific Symposium on Structural Reliability and Its Applications (APSSRA2020)
October 4–7 2020, Tokyo, Japan
T. Takada, I. Yoshida & T. Itoi (editors)

Insensitivity of Risk-Targeted Seismic Design Loads for Building Codes to the Requisite Fragility Curve Shape

N. Luco[1]

[1]*U.S. Geological Survey. Email: nluco@usgs.gov*

Abstract: Risk-targeted seismic design loads have been adopted in U.S. building codes, as have risk-targeted snow loads. Unlike the uniform-hazard loads in past building codes in the United States, building codes in most other countries, and design specifications for most non-building structures, risk-targeted seismic loads make use of a range of return periods on earthquake ground motion hazard curves. The range of ground motion return periods is dictated by a fragility curve shape of conditional probabilities of structural failure as a function of ground motion intensity. For the risk-targeted ground motions in U.S. building codes, the fragility curve shape is based on tens of thousands of nonlinear dynamic response simulations for buildings designed in accordance with the code provisions. For other potential risk-targeted loads, e.g., ground motions for bridge design, typically a comparable basis does not yet exist. Even for the simulation-based fragility curve shape, empirical evidence suggests that it overestimates the probabilities of failure. To inform improvements to this fragility curve shape and development of risk-targeted design loads for bridges and other applications, including other natural hazards, this paper quantifies the sensitivity of risk-targeted ground motions to the requisite fragility curve shape. Using nine such shapes and ground motion hazard curves for 34 city locations, 2 shear-wave velocities, and 3 spectral periods, I demonstrate that the risk-targeted loads are relatively insensitive to the fragility curve shape when the targeted risk is back-calibrated to risks resulting from the ground motions of the current design specifications.

Keywords: natural hazards, building codes, risk-targeted design loads, fragility curves, hazard curves, earthquakes.

1. Background

Since 2009, "Risk-Targeted" Maximum Considered Earthquake ground motion maps have been adopted for the seismic design loads of the *NEHRP Recommended Seismic Provisions for New Buildings and Other Structures* (National Earthquake Hazards Reduction Program, 2009, 2015, 2020, which are freely available online), the *ASCE 7 Standard, Minimum Design Loads and Associated Criteria for Buildings and Other Structures* (American Society of Civil Engineers, 2010, 2016), the *International Building Code* (International Code Council, 2012, 2015, 2018), and thereby local building codes throughout the United States.

Whereas the seismic maps of prior editions of these building code documents used "uniform-hazard" ground motions at a chosen return period, the risk-targeted maps are calculated for a targeted annualized frequency of building collapse (Luco et al., 2007). The risk-targeted maps make use of ground motions at all the return periods of seismic hazard curves, but also require a fragility curve shape of conditional collapse probabilities versus ground motions. For the building code documents mentioned above, the fragility curve shape is based on the Federal Emergency Management publication *FEMA P-695, Quantification of Building Seismic Performance Factors* (Applied Technology Council, 2009).

2. Motivation

Other building code documents in the United States and elsewhere are currently considering adopting risk-targeted seismic maps, e.g., the *American Association of State Highway Transportation Officials (AASHTO) Load and Resistance Factor Design (LRFD) Bridge Design Specifications* (as discussed in Murphy et al., 2020) and the *New Zealand Standards (NZS) 1170 Structural Design Actions* (written communication with Gerstenberger & Elwood, 2020), among several others. In general, the developers of such documents already have the requisite ground motion hazard curves (e.g., from Petersen et al., 2020 and Sterling et al., 2012), but do not yet have a basis like *FEMA P-695* for the structural fragility curve shape. The *FEMA P-695* project (a.k.a., Applied Technology Council, ATC-63) carried out tens of thousands of nonlinear dynamic response simulations for buildings designed to then-current code documents. Even for this simulation-based fragility curve shape, empirical evidence suggests that the true conditional probabilities of collapse might be smaller (e.g., Kircher et al., 2018). For both improving such fragility curve shapes and developing new risk-targeted design loads for building codes, whether for earthquakes or other hazards (e.g., Liel et al., 2017), quantifying the sensitivity of the risk-targeted loads to fragility curve shapes is important.

3. Objective

To specifically inform (i) improvements to the risk-targeted maps in future editions of the *NEHRP Recommended Seismic Provisions for New Buildings and Other Structures* and its downstream building code documents, and (ii) development of risk-targeted maps for future editions of the *AASHTO LRFD Bridge Design Specifications* and the *AASHTO Guide Specifications for LRFD Seismic Bridge Design*, here I quantify the sensitivity of risk-targeted ground motions to the requisite fragility curve shape. More generally, this sensitivity, or lack thereof, can also inform the adoption of risk-targeted maps for other building code documents in the United States and elsewhere.

4. Approach

The calculation of a risk-targeted ground motion from a hazard curve and fragility curve shape is iterative (Luco et al., 2007) and uses the so-called risk integral (e.g., Applied Technology Council, 1978), which can be expressed in two equivalent forms:

$$R = \int_0^\infty Fr(a|a_M) \cdot \frac{dH(a)}{da}\, da \quad (1a)$$

$$R = \int_0^\infty \frac{dFr(a|a_M)}{da} \cdot H(a)\, da \quad (1b)$$

where R denotes the risk (e.g., annualized frequency of building collapse); $Fr(a|a_M)$ denotes the fragility curve (e.g., conditional probability of collapse given each ground motion spectral acceleration, a), which in this application depends on the mapped ground motion, a_M; and $H(a)$ denotes the hazard curve (e.g., annualized frequency of exceeding each a). After setting the risk to a target value (e.g., 2.0E-4/year for the current *NEHRP Provisions*), a risk-targeted a_M is calculated through iterative application of Eq. 1a or 1b. The iteration finds the risk-targeted a_M corresponding to a fragility curve that, when integrated with the hazard curve, results in the targeted risk. The ensuing three subsections describe the hazard curves, fragility curve shapes, and risk targets I use in this paper.

4.1 Hazard curves

As the most recent ground motion hazard curves for the United States, I use those from the 2018 U.S. Geological Survey (USGS) National Seismic Hazard Model (NSHM; Petersen et al., 2020; Shumway et al., 2020). These hazard curves have been used for the 2020 edition of the *NEHRP Provisions* and are being considered for the next edition of the *AASHTO Specifications*. The hazard curves are for a 0.05-degree grid of locations that cover the conterminous United States, but for brevity, here I use only those for locations in 34 high-risk (i.e., high-hazard and/or large-population) cities that are considered as examples in the *NEHRP Provisions*. Furthermore, the 2018 USGS NSHM produced hazard curves for eight time-averaged 30-m shear-wave velocities (V_{S30}'s) ranging from 150 m/s to 1,500 m/s and 22 spectral acceleration periods ranging from 0 s to 10 s. Again, for brevity, here I use the hazard curves for V_{S30}'s of 760 m/s and 260 m/s, corresponding to NEHRP site classes BC and D, which are representative of reference and default site conditions. The spectral periods I use are 0.2 s, 1 s, and 5 s, which span the range used for the ground motion maps of the *2020 NEHRP Provisions*. The 34 locations, 2 shear-wave velocities, and 3 spectral periods are summarized in Table 1.

Table 1. Locations, shear-wave velocities (V_{S30}'s), and spectral periods of the subset of 2018 USGS NSHM hazard curves used.

Locations	34 from Table C11.4-1 of (NEHRP, 2009)
V_{S30}'s	760 m/s and 260 m/s
Spectral Periods	0.2 s, 1 s, and 5 s

4.2 Fragility curve shapes

The shape of the requisite fragility curve I use is defined in the *NEHRP Provisions* as a lognormal cumulative distribution function parameterized by (i) the conditional probability of collapse at the mapped ground motion, denoted here as p, and (ii) the logarithmic standard deviation of the distribution, denoted as β. In the 2009 edition of the *NEHRP Provisions*, p and β were set equal to 0.1 and 0.8, respectively. Subsequently, in the *2010 ASCE 7 Standard* and later editions of the *NEHRP Provisions*, β was changed to 0.6 based on expert opinion and *FEMA P-695*. This change alone, without changes to p and the risk target, was seen to typically result in less than 10% changes to the risk-targeted ground motions (Luco et al., 2015). Nevertheless, to quantify any interactions with changes to p, here I consider β's of 0.4, 0.6, and 0.8. More importantly, I also consider p's of 0.01, 0.1, and 0.2. The p of 0.01 explores potential improvements for the *NEHRP Provisions*. The p of 0.2 then brackets a range of potential values for the *AASHTO Specifications*, which might focus on a failure mode that is more likely than collapse. For example, the *2016 ASCE 7 Standard* also considers component or anchorage failure with a p as large as 0.25, although not for ground motion mapping. The fragility curve shapes corresponding to the nine pairs of p and β considered are shown in Fig. 1. Note that β changes the slope of the fragility curve and p changes the intercept with the mapped ground motion.

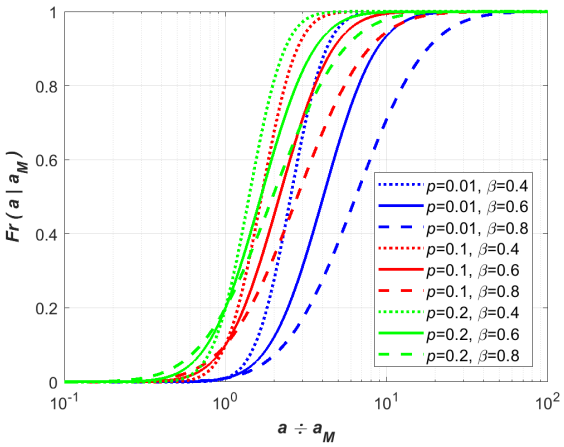

Figure 1. Fragility curve shapes and parameters considered.

4.3 Risk targets

For the 2009 edition of the *NEHRP Provisions*, the target annualized frequency of building collapse was set by "Project '07" (Kircher et al., 2010). It was back-calibrated to risks resulting from uniform-hazard ground motion maps at a return period of 2,475 years (see Luco et al., 2007 for details). These risks were calculated using the risk integral (Eq. 1), the selected fragility curve parameters (p=0.1, β=0.8), and the then-current mapped ground motions (a_M's) and hazard curves. Here, I take an analogous approach for each of the nine pairs of fragility parameters in Fig. 1 and calculate the risks resulting from the current mapped ground motions described below. The hazard curves used are those summarized in Table 1. Note that, in the future, the target risk might be based on comparisons with other natural hazards (e.g., hurricanes/typhoons), as well as input from policymakers, particularly if the risk is expressed in more universal terms like annualized fatalities. Until then, back-calibrating to the risks resulting from current maps is often preferable.

For informing potential improvements to the seismic maps of the *NEHRP Provisions*, I first calculate the risks

resulting from the risk-targeted ground motions of the current *2020 NEHRP Provisions* across the 34 city locations, 2 shear-wave velocities, and 3 spectral periods from Table 1. Each of these 204 ground motions, taken as a value of a_M, results in nine fragility curves from the shapes in Figure 1. Each of these fragility curves is then integrated with the respective hazard curve for the location, shear-wave velocity, and spectral period to calculate the risk via Eq. 1. The range and average of the 204 risk values for each pair of fragility parameters are summarized in Table 2. As expected, the average risk increases with p. When p=0.2, the average risk increases with β, as would be expected were p=0.5, the customary parameterization of the lognormal cumulative distribution function. When p=0.1, this expected increase with β is offset by the corresponding decreases in $Fr(a|a_M)$ seen in Figure 1; as a net result, the average risk only slightly differs with β. When p=0.01, the decreases in $Fr(a|a_M)$ dominate, resulting in the average risk decreasing with β.

Analogous to what Project '07 did for the *2009 NEHRP Provisions*, here I set the risk target for each pair of fragility curve parameters as equal to the corresponding average risk in Table 2. For p=0.1 and β=0.6, this target is equal to that of the *NEHRP Provisions*, which uses these same values of the fragility parameters for its risk-targeted ground motions. For the other potential fragility parameter values, the targets are different in order to back-calibrate to the corresponding risks resulting from the ground motion maps currently in the *NEHRP Provisions*.

Table 2. Risks (annualized frequencies of building collapse) resulting from the risk-targeted ground motions of the *2020 NEHRP Provisions*, across the locations, shear-wave velocities, and spectral periods summarized in Table 1.

Fragility Parameters	Risk Range	Risk Average
p=0.01, β=0.4	1.9E-5 to 1.3E-4	7.2E-5
p=0.01, β=0.6	1.7E-5 to 7.3E-5	4.0E-5
p=0.01, β=0.8	2.1E-5 to 4.7E-5	2.9E-5
p=0.1, β=0.4	1.4E-4 to 2.5E-4	2.2E-4
p=0.1, β=0.6	2.0E-4 to 2.0E-4	2.0E-4
p=0.1, β=0.8	1.7E-4 to 3.1E-4	2.1E-4
p=0.2, β=0.4	2.9E-4 to 3.6E-4	3.4E-4
p=0.2, β=0.6	2.9E-4 to 4.8E-4	3.7E-4
p=0.2, β=0.8	2.8E-4 to 8.1E-4	4.5E-4

For informing potential development of risk-targeted seismic maps for the *AASHTO Specifications*, I set the risk target for each potential pair of fragility parameters with the same approach as for the *NEHRP Provisions*, with one difference. Since the current *AASHTO Specifications* (2015, 2020) map uniform-hazard ground motions at a return period of 1,033 years (i.e., an exceedance probability of 7% in 75 years), here the target is set equal to the average risk resulting from 1,033-year ground motions of the 2018 USGS NSHM. Although this average is across the same 34 city locations, 2 shear-wave velocities, and 3 spectral periods used above, the differences between the uniform-hazard ground motions of the *AASHTO Specifications* and the risk-targeted ground motions of the *NEHRP Provisions* result in different risk, as summarized in Table 3. For a given pair of fragility parameters, the average risks for the *AASHTO Specifications* are higher because the 1,033-year ground motions are lower than the risk-targeted ground motions of the *NEHRP Provisions* (Luco et al., 2017).

Like for the *NEHRP Provisions*, the risk targets from Table 3 (set equal to the average risks) change with the fragility curve parameters in order to back-calibrate to the ground motion maps currently in the *AASHTO Specifications*. The risk target increases with p, increases slightly with β when p=0.2, only slightly differs with β when p=0.1, and decreases with β when p=0.01, for the same reasons explained above for Table 2.

Table 3. Risks (annualized frequencies of failure) resulting from 1,033-year ground motions like those of the current *AASHTO Specifications*, across the locations, shear-wave velocities, and spectral periods summarized in Table 1.

Fragility Parameters	Risk Range	Risk Average
p=0.01, β=0.4	6.2E-5 to 3.6E-4	1.6E-4
p=0.01, β=0.6	4.6E-5 to 2.2E-4	9.1E-5
p=0.01, β=0.8	4.3E-5 to 1.4E-4	6.3E-5
p=0.1, β=0.4	3.6E-4 to 6.0E-4	4.4E-4
p=0.1, β=0.6	3.3E-4 to 4.9E-4	3.9E-4
p=0.1, β=0.8	3.2E-4 to 6.0E-4	3.9E-4
p=0.2, β=0.4	6.0E-4 to 7.3E-4	6.5E-4
p=0.2, β=0.6	5.8E-4 to 9.9E-4	6.7E-4
p=0.2, β=0.8	5.6E-4 to 1.5E-3	7.8E-4

5. Results for *NEHRP Provisions*

With the approach described in the preceding section, here I calculate risk-targeted ground motions (RTGMs) using the nine fragility curve shapes (i.e., pairs of p and β values) considered in this sensitivity study (see Fig. 1). For each fragility curve shape, the RTGMs are calculated for the aforementioned 34 city locations, 2 shear-wave velocities, and 3 spectral periods, generating a total of 204 RTGMs. Before calculating the RTGMs for the back-calibrated risk targets from Table 2, I first do the calculations with the current risk target of the *NEHRP Provisions*, namely an annualized frequency of building collapse of 2.0E-4/year. The sensitivity of these initial RTGMs to the fragility curve shape provides a baseline for the sensitivity with back-calibrated risk targets.

5.1 Sensitivity using fixed risk target

With the risk target of 2.0E-4/year, Fig. 2 summarizes the percent changes in the RTGMs calculated using the various fragility curve shapes relative to those calculated using the shape currently in the *NEHRP Provisions* (i.e., p=0.1 and β=0.6). The figures present box-and-whisker plots (a.k.a., boxplots) of the RTGM percent changes. The central red line of each boxplot illustrates the median percent change, the blue box illustrates the interquartile range of percent changes (from the 25th to 75th percentiles), the black whiskers illustrate the extreme changes not considered outliers, and the red plus signs illustrate the outliers, which are changes more than 1.5 times the interquartile range away from the edges of this range.

The RTGM sensitivity to β alone is illustrated in the two upper-left boxplots of Fig. 2. The median percent changes in RTGM when using β=0.4 and β=0.8 are less

than +5% relative to those using β=0.6. Even the full ranges (whiskers) of the percent changes are within approximately -10% to +15%. This insensitivity of RTGMs to β is in line with the results of Luco et al. (2015) that were mentioned above in Section 4.2.

The sensitivity to p alone is illustrated in the two upper-right boxplots of Fig. 2. From p=0.1 to p=0.01, the RTGMs change by approximately -45%. This is because, with a given risk target, a less fragile structure (in this case p=0.01) allows for smaller RTGMs. Without back-calibrated risk targets, this sensitivity of RTGMs to p is expected. Correspondingly, from p=0.1 to p=0.2, the RTGMs change by approximately +30%, because a more fragile structure calls for larger RTGMs. The absence of variability about the median percent change when p alone is changed, without a change to β, is explained below with the results for the *AASHTO Specifications*.

The sensitivity to changes in β and p at the same time, still without back-calibrated risk targets, is illustrated in the bottom four boxplots of Fig. 2. From the median percent changes when β=0.4 (i.e., -30% for p=0.01 and +25% for p=0.2), we see that the RTGMs are less sensitive to p than when β=0.8 (see median percent changes of -55% for p=0.01 and +45% for p=0.2). In the limit, as β approaches zero, one would expect the fragility curve shapes and hence the RTGMs to become insensitive to p.

5.2 Sensitivity using back-calibrated risk targets

With the back-calibrated risk targets from Table 2, the RTGM sensitivity to the fragility curve shape is presented in Fig. 3. There, the median percent changes in RTGM relative to the current fragility curve parameters of the *NEHRP Provisions* (i.e., p=0.1 and β=0.6) are all near zero. However, there is some variability about the median percent changes, because the back-calibrated risk targets are only averages of the risks across the 34 city locations, 2 shear-wave velocities, and 3 spectral periods. The interquartile ranges of percent changes are all within approximately ±10%. The full ranges (whiskers) of changes are within approximately ±30%. The outliers, all above +30% but below +40%, are when p=0.01 at 2 of the 34 city locations: Charleston (South Carolina), where the shapes of the hazard curves are notably different than the other locations, and New York City, where the RTGMs and hence their absolute differences (as opposed to percent changes) are relatively small. These outlying RTGM changes are smaller than the *median* -55% to -45% changes without back-calibrated risk targets (from Fig. 2). They are also smaller than some of the changes in mapped ground motions from one edition of the *NEHRP Provisions* to the next (Luco et al., 2015). More observations from Fig. 3 are discussed below with the results for the *AASHTO Specifications*.

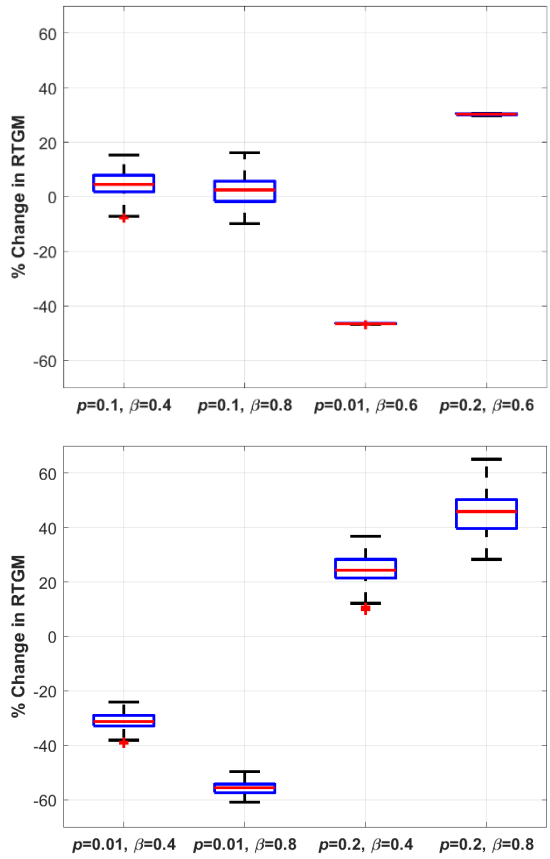

Figure 2. Boxplots of percent changes in risk-targeted ground motions relative to those calculated using the current fragility curve parameters of the *NEHRP Provisions* (p=0.1, β=0.6), with the current risk target (2.0E-4/year).

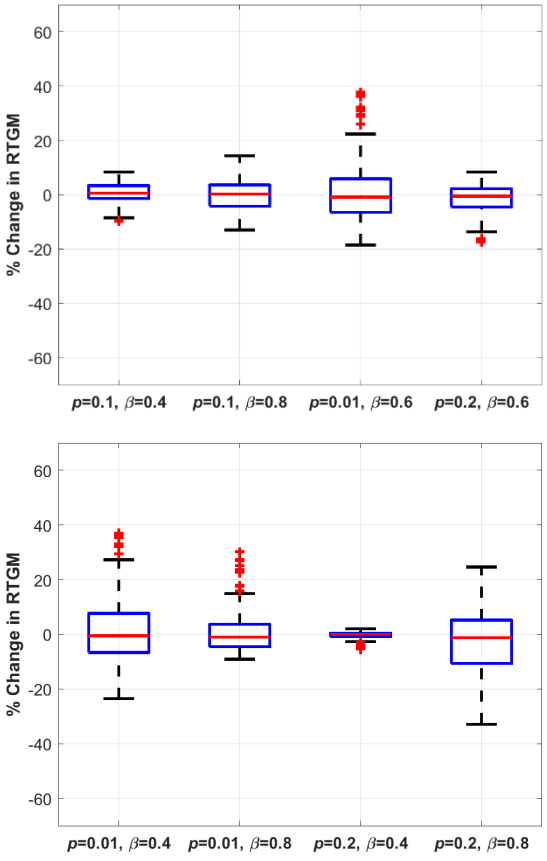

Figure 3. Boxplots of percent changes in risk-targeted ground motions relative to those calculated using the current fragility curve parameters of the *NEHRP Provisions* (p=0.1, β=0.6), with back-calibrated risk targets (from Table 2).

6. Results for *AASHTO Specifications*

To inform potential development of risk-targeted maps for future editions of the *AASHTO Specifications*, here I quantify RTGM sensitivity with the same approach as in the preceding section, but with one difference. Here, the risk targets are from Table 3, i.e., those back-calibrated to uniform-hazard ground motions at the current 1,033-year return period of the *AASHTO Specifications*. For the initial RTGMs calculated using a fixed risk target across the various fragility curve shapes, I use the risk target back-calibrated with the fragility curve parameters p=0.1 and β=0.6. I also use these "base case" parameters for the RTGMs from which percent changes are calculated. These consistencies with the preceding section allow me to attribute any differences in the sensitivity results to the differences between the ground motions of the *AASHTO Specifications* and *NEHRP Provisions*.

6.1 Sensitivity using fixed risk target

With the risk target from the row of Table 3 that corresponds to p=0.1 and β=0.6, namely 3.9E-4/year, the percent changes in RTGMs are nearly the same as those shown in Fig. 2 above. In lieu of a figure of this similar RTGM sensitivity for the *AASHTO Specifications*, here I explain why it is so similar to that for the *NEHRP Provisions*.

Starting with the RTGM sensitivity to p alone (i.e., the two upper-right boxplots of Fig. 2), the absence of variability about the median percent change can be explained via an approximate closed-form solution of the risk integral (Eq. 1). The approximate "risk equation" (e.g., see Appendix F of McGuire, 2004) assumes a linearly shaped hazard curve in logarithmic space (for both axes) and the same lognormally shaped fragility curve used in the *NEHRP Provisions* and this paper. With these assumptions, the percent change in RTGM when only p changes, from p_0 to p_1, can be calculated as

$$C = \left(e^{-\beta[\Phi^{-1}(p_1)-\Phi^{-1}(p_0)]} - 1\right) \cdot 100\% \qquad (2)$$

where C denotes the percent change and $\Phi^{-1}(p)$ is the inverse of the standard normal cumulative distribution function (e.g., $\Phi^{-1}(0.1)$ = -1.28). As this equation only depends on β and the two values of p, it suggests that the percent change does not vary across the city locations, shear-wave velocities, and spectral periods, consistent with Fig. 2. It also suggests that the corresponding percent change for the *AASHTO Specifications* is the same as that for the *NEHRP Provisions*; although not shown here, this is indeed the case.

Regarding the RTGM sensitivity to changes in β alone or in β and p at the same time, still with a fixed risk target, the variability about the median percent change seen in the corresponding boxplots of Fig. 2 can likewise be explained via the approximate risk equation. An analog to Eq. 2 suggests that the percent change also depends on the slope of the hazard curve (in addition to β and p), which varies with the city location, shear-wave velocity, and spectral period. Although not shown here, the hazard curve slopes near the ground motions of the *AASHTO Specifications* are similar to those of the *NEHRP Provisions*, which explains the similarity of the RTGM sensitivities.

6.2 Sensitivity using back-calibrated risk targets

With the back-calibrated risk targets of Table 3, the percent changes in RTGMs across the various fragility curve shapes are again nearly the same as those for the *NEHRP Provisions* (shown in Fig. 3 above). As in the preceding subsection, the similarities can be explained via the approximate closed-form solution of the risk integral. In lieu of these details or a figure of the similar RTGM sensitivity for the *AASHTO Specifications*, here I explain why the variabilities about the median percent changes in Fig. 3 differ with the fragility curve parameters.

While the median percent changes in RTGM relative to the base case fragility parameters (p=0.1, β=0.6) are all near zero, the variability about the median is smallest when p=0.2 and β=0.4. The fragility curve shapes for these two pairs of parameters explain why. Whereas Fig. 1 shows the shapes across a wide range of ground motions, Fig. 4 shows them where they contribute most to the risk, near the RTGM (i.e., near $a \div a_M$=1). Fig. 4 also normalizes the ordinates of the fragility curve shapes by their value at the RTGM (i.e., p). The figure reveals that when p=0.2 and β=0.4, the shape is closest to the base case of p=0.1 and β=0.6. Conversely, the shapes for (p=0.01, β=0.4), (p=0.01, β=0.6), and (p=0.2, β=0.8) are farthest from the base case. Correspondingly, the variabilities of the percent changes in Fig. 3 are largest for these three pairs of fragility parameters.

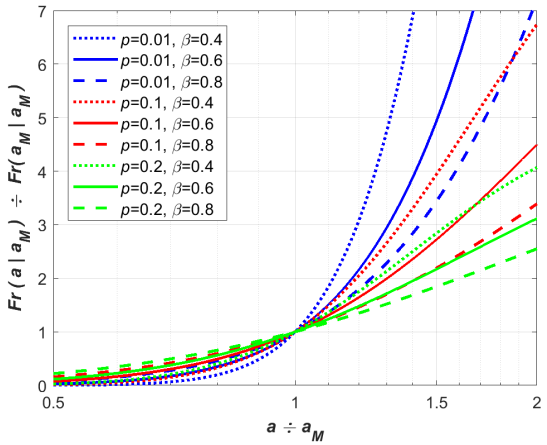

Figure 4. Zoomed-in view of Fig. 1, with the ordinates of the fragility curve shapes normalized by their value at the RTGM.

7. Conclusions

To inform potential improvements to the fragility curve shape used in the *NEHRP Provisions* and potential development of risk-targeted ground motions (RTGMs) for the *AASHTO Specifications*, this paper quantifies the sensitivity of RTGMs to the parameters of the fragility curve shape. When a fixed risk target is used, like the current annualized frequency of collapse of the *NEHRP Provisions* (2.0E-4), the median percent change in the RTGM from the base case parameters is as large as -55% (see Fig. 3). However, when the risk targets are back-calibrated to the average risk resulting from the current ground motions of the *NEHRP Provisions* (Table 2) and

AASHTO Specifications (Table 3), the median percent change in RTGM is near zero for all of the various fragility curve parameters (see Fig. 4). The variability about each of these medians depends on how different the fragility curve shapes are near the RTGM, but for the range of shapes considered in this paper, overall the RTGMs using back-calibrated risk targets are relatively insensitive to the fragility curve parameters.

9. Acknowledgments

Thank you to reviewers Lee Marsh of WSP USA; Jose Restrepo and Joel Conte of the University of California San Diego; and Sanaz Rezaeian, Mark Petersen, Jill McCarthy, and Janet Slate of the U.S. Geological Survey.

References

American Association of State Highway Transportation Officials. 2020. *AASHTO LRFD Bridge Design Specifications, 9th Edition.* Washington, D.C.

American Association of State Highway Transportation Officials. 2015. *AASHTO Guide Specifications for LRFD Seismic Bridge Design, 2nd Edition.* Washington, D.C.

American Society of Civil Engineers, Structural Engineering Institute. 2010. *Minimum Design Loads for Buildings and Other Structures*, ASCE/SEI 7-10.

American Society of Civil Engineers, Structural Engineering Institute. 2016. *Minimum Design Loads for Buildings and Other Structures,* ASCE/SEI 7-16.

Applied Technology Council. 1978. *Tentative Provisions for the Development of Seismic Regulations for Buildings,* ATC 3-06.

Applied Technology Council. 2009. Quantification of Building Seismic Performance Factors. *Federal Emergency Management Agency Publication*, FEMA P-695.

Gerstenberger, M. and Elwood, K. 2020. *Written communication*.

International Code Council. 2012. *International Building Code*. Falls Church, Virginia.

International Code Council. 2015. *International Building Code*. Falls Church, Virginia.

International Code Council. 2018. *International Building Code*. Falls Church, Virginia.

Kircher, C.A., Luco, N. and Whittaker, A.S. 2010. Project 07—Reassessment of Seismic Design Procedures, *Proceeding of the Structures Congress 2010,* Orlando, Florida.

Kircher, C.A., Pang. W., Ziaei, E., Filiatrault, A. and Heintz, J. 2018. Solutions to the short-period building performance paradox. *Proceedings of the 11th U.S. National Conference on Earthquake Engineering,* Los Angeles, California.

Liel, A.B., DeBock, D.J., Harris, J.R., Ellingwood, B.R. and Torrents, J.M. 2017. Reliability-based Design Snow Loads, II: Reliability Assessment and Mapping Procedures. *Journal of Structural Engineering,* 143(7).

Luco, N., Ellingwood, B.R., Hamburger, R.O., Hooper, J.D., Kimball, J.K. and Kircher, C.A. 2007. Risk-targeted versus current seismic design maps for the conterminous United States. *Proceedings of the Structural Engineers Association of California 76th Annual Convention*, Lake Tahoe, California.

Luco, N., Bachman, R.E., Crouse, C.B., Harris, J.R., Hooper, J.D., Kircher, C.A., Caldwell, P.J. and Rukstales, K.S. 2015. Updates to Building-code Maps for the 2015 NEHRP Recommended Seismic Provisions. *Earthquake Spectra*, 31(S1).

Luco, N., Liu, T.J. and Rukstales, K.S. 2017. A risk-targeted alternative to deterministic capping of maximum considered earthquake ground motion maps. *Proceeding of the 16th World Conference on Earthquake Engineering*, Santiago, Chile.

McGuire, R.K. 2004. Seismic Hazard and Risk Analysis. *Earthquake Engineering Research Institute Monograph*, MNO-10.

Murphy, T., Marsh, L., Bennion, S., Buckle, I.G., Luco, N., Anderson, D., Kowalsky, M. and Restrepo, J. 2020. Proposed Guidelines for Performance-based Seismic Bridge Design. *National Cooperative Highway Research Program Report*, Washington, D.C.

National Earthquake Hazards Reduction Program. 2009. NEHRP Recommended Seismic Provisions for New Buildings and Other Structures. *Federal Emergency Management Agency Publication*, FEMA P-750, https://www.fema.gov/media-library/assets/documents/18152.

National Earthquake Hazards Reduction Program. 2015. NEHRP Recommended Seismic Provisions for New Buildings and Other Structures, Volume 1: Part 1 Provisions, Part 2 Commentary. *Federal Emergency Management Agency Publication*, FEMA P-1050-1, https://www.fema.gov/media-library/assets/documents/107646.

National Earthquake Hazards Reduction Program. 2020. NEHRP Recommended Seismic Provisions for New Buildings and Other Structures, Volume 1: Part 1 Provisions, Part 2 Commentary. *Federal Emergency Management Agency Publication*, FEMA P-2082-1.

Petersen, M.D., Shumway, A.M., Powers, P.M., Mueller, C.S., Moschetti, M.P., Frankel, A.D., Rezaeian, S. McNamara, D.E., Luco, N., Boyd, O.S., Rukstales, K.S., Jaiswal, K.S., Thompson, E.M., Hoover, S.M., Clayton, B.S., Field, E.H. and Zeng, Y. 2020. The 2018 update of the US National Seismic Hazard Model: Overview of model and implications. *Earthquake Spectra*, 36(1).

Shumway, A.M., Clayton, B.S. and Rukstales, K.S. 2020. Data release for additional period and site class data for the 2018 National Seismic Hazard Model for the conterminous United States. *U.S. Geological Survey data release,* https://doi.org/10.5066/P9RQMREV.

Stirling, M., McVerry, G., Gerstenberger, M., Litchfield, N., Van Dissen, R., Berryman, K., Barnes, P., Wallace, L. Villamor, P., Langridge, R., Lamarche, G., Nodder, S., Reyners, M., Bradley, B., Rhoades, D., Smith, W., Nicol, A., Pettinga, J., Clark, K. and Jacobs, K. 2012. National Seismic Hazard Model for New Zealand: 2010 Update. *Bulletin of the Seismological Society of America*, 102(4).